JOURNAL OF MATERIALS SCIENCE 31 (1996) 5631–5641

Detailed analysis of the fibre pull-out test

A. ZUCCHINI
ENEA, INN.FIS.MACO, C.R.E. "E. Clementel", V. Don Fiammelli, 2, 40129 Bologna, Italy
C. Y. HUI
Theoretical and Applied Mechanics, Cornell University, 224 Kimball Hall, Ithaca, NY 14853, USA

A detailed finite element analysis has been carried out to simulate the fibre pull-out test. The fibre–matrix interface was assumed to obey a Coulomb friction law. Special attention was focused on the effect of residual thermal stresses. An approximate analytical solution, rather similar to those in the literature, was derived. The results of the finite element analysis have been used to investigate the limitation and the validity of this analytical solution. The accuracy of various approximate analyses has also been discussed.

1. Introduction

The control of adhesion between the fibre–matrix interface in fibre-reinforced composites is of paramount importance in determining the usefulness of these materials. If the interface cracks too easily, the elastic and compressive strength properties of the composite are compromised. On the other hand, if the interface is too strong, cracks may run easily through the composite without being deflected along the fibre interfaces, thus compromising the fracture toughness of the composite.

A practical measure of the ability of the fibre–matrix interface to transfer load is the interface shear strength, τ. The tests most often used to determine τ are the single-filament fragmentation test [1–3], the fibre push-out test [4–7] and the fibre pull-out test [8–12]. In the fibre pull-out test, a single fibre is pulled out of a block of matrix material in which it is partially embedded. The fibre load and the relative displacement (the slip) at the fibre–matrix interface are measured. The test is often interpreted by assuming that the shear resistance at the fibre–matrix interface is characterized by a constant frictional shear stress, τ.

The mechanics of the fibre pull-out test have been considered by many investigators in various degrees of sophistication. Starting with the simple shear-lag analysis of Cox [13], more elaborate approximate analyses have been proposed to solve a wide variety of load-transfer problems involving bimaterial interfaces of which the fibre pull-out test is a special case [14–16]. These approximate methods have been used extensively to obtain analytical solutions for the fibre pull-out test [17–30]. For example, Takaku and Arridge [19] introduced a modified shear-lag analysis that accounts approximately for the variation in the interface normal stress which accompanies Possion contraction of the pulled fibre. The effect of residual stresses on the pull-out test was investigated by Kerans and Parthasarathy [29]; they use a modified shear-lag analysis which accounts for both the axial and radial residual stresses. Steif and Hoysan [24] have obtained a highly accurate, detailed numerical solution of a two-dimensional analogue of the pull-out problem. The residual stresses in their calculation, however, are simulated by a far-field compressive stress, so that the effect of axial residual stress is absent in their analysis. Although there are many analytical solutions for the pull-out tests [17–30], there have been very few attempts to verify the accuracy of these analytical solutions which are based mostly on modified shear-lag models. Amongst the few numerical simulations of the pull-out test, for example [24], the thermal residual stresses are not explicitly included in the numerical computations.

The purpose of the present study was to assess the accuracy of the approximate shear-lag analysis by comparing the analytical results with detailed finite element simulation of the pull-out test. Specifically, the accuracy of the analytical solution depends on the elastic properties of the fibre and the matrix, the friction coefficient and the geometry of the specimen. Our goal was to illucidate the regime of validity of the shear-lag model using an accurate numerical method. The residual stress calculation has been explicitly included in the finite element model. The analytical formulation presented here is a modified shear-lag analysis with results similar to those derived by Kerans and Parthasarathy [29] and Li and Grubb [30]. The axial residual stress, which affects the friction force acting on the interface, is included explicitly in the analysis.

2. Analytical modelling of fibre pull-out

The geometry of the fibre pull-out test is shown schematically in Fig. 1. The specimen is a circular cylinder with radius R_m and thickness t. A circular fibre with radius R_f is pulled out from the matrix with a uniform normal traction $\sigma_z = p$ applied at its end. To obtain

0022–2461

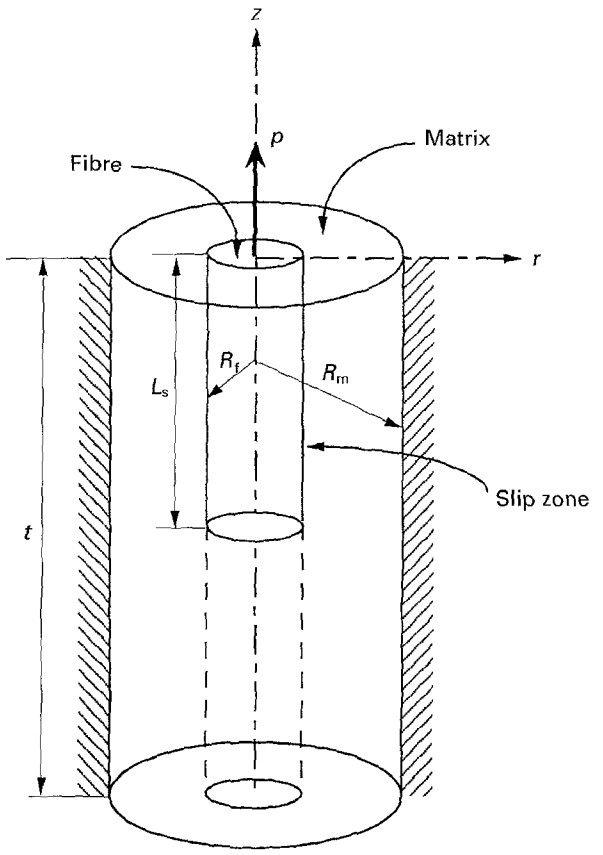

Figure 1 Schematic drawing of the fibre pull-out test. The boundary $r = R_m$ is clamped. The circular fibre with radius R_f is pulled-out from the matrix with a uniform normal stress $\sigma_z = p$. The rest of the boundary is traction free.

an approximate analytical solution of this problem, we assume that $t \to \infty$ and $R_m \to \infty$. In other words, the matrix occupies the lower half space $z < 0$. The problem is axisymmetric about the fibre axis which is in the z direction. The fibre–matrix interface is located at $r = R_f$ and $z < 0$. Traction-free boundary condition is imposed on the surface $r > R_f$ and $z = 0$. Both the matrix and fibre are assumed to be linearly elastic and isotropic with Young's modulus and Poisson's ratio (E_m, ν_m) and (E_f, ν_f), respectively.

2.1. Thermal stress problem

Residual stresses in the pull-out specimen are generated due to the difference in the thermal coefficient of expansion of the matrix and the fibre denoted by α_m and α_f, respectively. In the analytical model, this stress state is estimated using the residual stresses t_{ij}^f and t_{ij}^m, induced by cooling an infinitely long fibre embedded in an infinite matrix by ΔT, where ΔT is the difference between the temperature of the stress-free state and the test temperature. The superscripts in t_{ij}^m and t_{ij}^f denote the thermal stresses in the matrix and the fibre, respectively. Note that the residual stresses t_{ij}^f estimated using this solution are approximate, as they do not satisfy the traction-free boundary condition on the surface $z = 0$.

The non-trivial fibre-stress components of t_{ij}^f are found to be [31]

$$t_R^f = t_\theta^f = \xi E_m(\alpha_m - \alpha_f)\Delta T \tag{1a}$$

$$t_z^f = t_R^f\left[1 + \frac{E_f(1 + \nu_m)}{E_m(1 + \nu_f)}\right] \tag{1b}$$

where

$$\xi \equiv \frac{E_f(1 + \nu_f)}{E_f(1 + \nu_m) + E_m(1 + \nu_f)(1 - 2\nu_f)} \tag{1c}$$

Equation 1 is expected to approximate the actual stress distribution in the fibre and the traction, t_R^f, on the fibre–matrix interface with the exception of a small region near the traction-free surfaces $z = 0$. The validity of this approximation will be examined by our finite element calculation in Section 3.

2.2. Analysis of pull-out

Following Meda *et al.* [32], we assumed that slip along the fibre matrix interface is governed by Coulomb friction. At any given instant in the loading history, either sticking, slipping or opening can occur at a point along the interface. Conditions for these three states are as follows:

(i) stick condition

$$\sigma_R < 0, \ |\sigma_{Rz}| < \mu|\sigma_R|, \quad \frac{dg}{dt} = \frac{dh}{dt} = h = 0$$

(ii) slip condition

$$\sigma_R < 0, \ |\sigma_{Rz}| = \mu|\sigma_R|,$$

$$\operatorname{sgn}\left(\frac{dg}{dt}\right) = \operatorname{sgn}(\sigma_{Rz}), \ h = \frac{dh}{dt} = 0$$

(iii) open condition

$$\sigma_R = \sigma_{Rz} = 0 \quad h > 0$$

where

$$g = \lim_{\varepsilon \to 0^+}[u_z(R_f + \varepsilon, z) - u_z(R_f - \varepsilon, z)]$$

$$h = \lim_{\varepsilon \to 0^+}[u_R(R_f + \varepsilon, z) - u_R(R_f - \varepsilon, z)]$$

where μ is the friction coefficient.

The residual thermal stresses, due to the cooling of the specimen from the stress-free temperature to the test temperature, are given by Equation 1. This assumption implies that the fibre end at $z = 0$ is compressed by a residual stress of $p = t_z^f$ before any external load is applied.

The following assumptions are made in the analytical solution.

(A) The fibre is modelled as a rod, i.e. the fibre stress is independent of r so that

$$\frac{\partial \sigma_R^f}{\partial r} = 0 \tag{2a}$$

$$\frac{\partial \sigma_z^f}{\partial r} = 0 \tag{2b}$$

(B) The effects of the shear stress σ_{Rz} on the displacement in the radial direction, u_R, is neglected in both the fiber and matrix, as in [32].

(C) We neglect the effects of the shear stress σ^f_{Rz} on u^f_z, so that u^f_z is independent of r, which is consistent with the rod assumption A.

For an axisymmetric problem with residual stresses, the stress–strain relations of the fibre in cylindrical coordinates are

$$\frac{\partial u^f_R}{\partial r} = \frac{\Delta\sigma^f_R - \nu_f \Delta\sigma^f_z - \nu_f \Delta\sigma^f_\theta}{E_f} \tag{3a}$$

$$\frac{\partial u^f_z}{\partial z} = \frac{\Delta\sigma^f_z - \nu_f \Delta\sigma^f_R - \nu_f \Delta\nu^f_\theta}{E_f} \tag{3b}$$

where the notation $\Delta\sigma^f_{ij} \equiv \sigma^f_{ij} - t^f_{ij}$ has been used. Note that the deformation is measured with respect to a specimen at the test temperature loaded at the end by a compressive stress $p = t^f_z$. This is because the residual stresses are obtained assuming that the fibre is infinite in the z direction. Equilibrium in the radial direction, i.e.

$$\frac{\partial \sigma_R}{\partial r} + \frac{\sigma_R - \sigma_\theta}{r} + \frac{\partial \sigma_{Rz}}{\partial z} = 0 \tag{4}$$

and assumption A implies that

$$\sigma^f_\theta = \sigma^f_R + r\frac{\partial \sigma^f_{Rz}}{\partial z} \tag{5}$$

Substituting Equation 5 into Equation 3a results in

$$u^f_R = \left[\frac{(1-\nu_f)\Delta\sigma^f_R - \nu_f \Delta\sigma^f_z}{E_f}\right] r \tag{6}$$

where we have ignored the term $\partial\sigma^f_{Rz}/\partial z$ in Equation 3a according to assumption B. The displacement on the matrix side is derived following Meda *et al.* [32] by assuming that the matrix is an infinite slab deforming under plane strain condition, with a hole of radius R_f subjected to an internal pressure $\Delta\sigma^m_R$

$$u^m_R = -\frac{(1+\nu_m)\Delta\sigma^m_R}{E_m} R_f \qquad \text{at } r = R_f \tag{7}$$

Note that assumption B is used in the derivation of Equation 7. Imposing radial displacement and traction continuity at the interface, i.e.

$$\begin{cases} u^f_R = u^m_R & \text{(8a)} \\ \qquad\qquad \text{at } r = R_f & \\ \Delta\sigma^f_R = \Delta\sigma^m_R & \text{(8b)} \end{cases}$$

Equations 6 and 7 imply that

$$\Delta\sigma^f_z = \frac{\Delta\sigma^f_R}{k} \tag{9a}$$

where

$$k \equiv \frac{\nu_f E_m}{(1+\nu_m)E_f + (1-\nu_f)E_m} \tag{9b}$$

Equation 9a gives the relationship between the normal stress acting on the fibre–matrix interface and the tensile stress on the fibre.

A slip zone is developed as load is applied to the fibre end at $z = 0$. Inside the slip zone, the Coulomb friction law, for $\sigma^f_R < 0$, is

$$\sigma_{Rz} = -\mu\sigma^f_R \tag{10}$$

The equilibrium of a fibre element in the slip zone is

$$\frac{\partial \sigma^f_z}{\partial z} = -\frac{2\sigma_{Rz}}{R_f} \tag{11}$$

Inserting Equations 9a and 10 in Equation 11 yields a first-order differential equation

$$\frac{\partial \Delta\sigma^f_z}{\partial z} = \frac{2\mu}{R_f}(t^f_R + k\Delta\sigma^f_z) \tag{12}$$

This equation is integrated with the boundary condition $\sigma^f_z = p$ at $z = 0$, leading to

$$\Delta\sigma^f_z = -\frac{t^f_R}{k} + \left(p - t^f_z + \frac{t^f_R}{k}\right)\exp\left(\frac{2k\mu}{R_f} z\right) \tag{13}$$

where p is the applied tension on the fiber end and is related to the pull-out force F by

$$F = \pi R^2_f p \tag{14}$$

Equation 13 gives the axial fibre stress for a point inside the slip zone. The length of the slip zone, L_S, is defined by the condition that no slip can occur beyond $z = L_S$.

Following Shetty [5] and Kerans and Parthasarathy [29], we require that

$$\Delta\sigma^f_z = 0 \qquad \text{at } z = L_S \tag{15}$$

Equation 15 states that the axial fibre stress just outside the slip zone is the residual axial stress. The error induced by this boundary condition is small, as long as the slip zone is large compared with the fibre radius. L_S is calculated using Equations 13 and 15 and is found to be

$$L_S = \frac{R_f}{2\mu k} \ln\left(\frac{t^f_R}{t^f_R - kt^f_z + kp}\right) \tag{16}$$

The axial displacement $u^f_z = u^f_z(z, p)$ is obtained by integrating Equation 3b subjected to the condition that $u^f_z(z = L_S, p) = 0$. The integration is carried out by inserting Equations 5, 9a and 13 into Equation 3b and neglecting the shear stress term $\partial\sigma^f_{Rz}/\partial z$ according to assumption C. This procedure allows us to determine the axial displacement of the fibre at $z = 0$

$$u^f_z(0, p) = \frac{1 - 2\nu_f k}{E_f}\left[(p - t^f_z)\frac{R_f}{2\mu k} + \frac{t^f_R}{k} L_S\right] \tag{17}$$

Note that $u^f_z(0, p)$ is non-zero when the applied stress p vanishes because the fibre is initially compressed on its free surface by the residual stress t^f_z due to the infinite fibre approximation.

The displacement u^f_z in our model is calculated with respect to the specimen in the residual stress state which is obtained using the infinite fibre approximation, the consequence of this approximation is that the fibre is initially compressed on its free surface by the residual stress t^f_z. On the other hand, the actual experimental displacement U_f at $z = 0$ is measured with respect to a residual stress state which obeys the traction-free boundary condition on the surface $z = 0$.

A good approximation of U_f is obtained by subtracting the displacement $u_z^f(0, 0)$ computed using Equation 17. In other words, we subtract the displacement $u_z^f(0, 0)$, due to the release of the excess residual stress near the fibre end, i.e.

$$U_f = u_z^f(0, p) - u_z^f(0, 0) \tag{18}$$

Using Equation 17, U_f is found to be

$$U_f = \frac{1 - 2\nu_f k}{E_f}\left(p\frac{R_f}{2\mu k} + \frac{t_R^f}{k}\Delta L_S^0\right) \tag{19a}$$

where

$$\Delta L_S^0 = L_S(p) - L_S(0) = \frac{R_f}{2\mu k}\ln\left(\frac{t_R^f - kt_z^f}{t_R^f - kt_z^f + kp}\right) \tag{19b}$$

Introducing the dimensionless variables

$$\bar{p} = \frac{k}{|t_R^f|}p \tag{20a}$$

$$\bar{u} = \frac{\mu k E_f}{pR_f}U_f \tag{20b}$$

$$\bar{p}_{cr} = 1 - k\frac{t_z^f}{t_R^f} \tag{20c}$$

where $|t_R^f| = -t_R^f$ for a residual compressive stress, we obtain

$$\bar{u} = \frac{(1 - 2\nu_f k)}{2}\left[1 + \frac{1}{\bar{p}}\ln\left(1 - \frac{\bar{p}}{\bar{p}_{cr}}\right)\right] \tag{21}$$

The slip length, in terms of the normalized variables, is found to be

$$L_S = -\frac{R_f}{2\mu k}\ln(\bar{p}_{cr} - \bar{p}) \tag{22}$$

Note that the normalized displacement, $\bar{u}$, given by Equation 21 is a non-linear function of the normalized load, $\bar{p}$, and is independent of μ. This means that the measured displacement, U_f, is inversely proportional to μ.

The interfacial shear stress, σ_{Rz}, inside the slip zone can be obtained from Equations 11 and 13; it is found to be

$$\sigma_{Rz} = \mu|t_R^f|(\bar{p}_{cr} - \bar{p})\exp\left(\frac{2\mu kz}{R_f}\right) \qquad 0 \leqslant z \leqslant L_S \tag{23a}$$

It is convenient to introduce a normalised interfacial shear stress, $\bar{\tau}$

$$\bar{\tau} \equiv \frac{\sigma_{Rz}}{\mu|t_R^f|} \tag{23b}$$

The axial fibre stress, σ_z^f, within the slip zone can be expressed in terms of a normalized fibre stress, $\bar{\sigma}$, as

$$\sigma_z^f = |t_R^f|(\bar{\sigma}/k) \tag{23c}$$

where

$$\bar{\sigma} \equiv (\bar{p}_{cr} - \bar{\tau}) \tag{23d}$$

Equation 21 implies that when the normalized tension, $\bar{p}$, reaches the "critical" value, $\bar{p}_{cr}$ (i.e. $p_{cr} = t_z^f - (t_R^f/k)$), the axial displacement becomes unbounded; this corresponds to the situation when the applied load is such that the radial stress due to Poisson's contraction exactly cancels the radial normal residual stress [29]. In other words, there is no frictional resistance to the external load. This corresponds to the propagation of a mode I crack and our analysis is no longer valid: a similar transition of the crack propagation from mode II to mode I has been found [27] and the existence of a critical load has also been observed [26]. Note that the applied tension, p, is normalized with respect to $|t_R^f|/k$, which is the stress needed to cancel the radial normal stress when no axial residual stress is present. Finally, we note that the normalized critical load $\bar{p}_{cr} = 1$ for the case when the axial residual stress is set to zero.

3. FEM analysis

The finite element analysis of the pull-out test is carried out using the code ABAQUS, developed by Hibbitt, Karlsson and Sorensen Inc. The geometry is shown in Fig. 1. The height, t, of the cylinder ranges between 10 and 100 fibre radii, R_f. The matrix radius, R_m, is chosen to be $60R_f$ to simulate the effect of an infinite matrix. The domain of interest is modelled by means of 500 biquadratic axisymmetric elements (8 nodes) and 20 interface elements (3 nodes).

Coulomb friction is used in the interface elements: if the normal stress acting on the two sides of the element is tensile, the two sides separate so that there is no normal and shear stress transfer between fibre and matrix. When the normal stress is compressive, the displacement across the interface is continuous up to the shear limit (the friction coefficient times the normal stress) with slip occurring between the interfaces at higher values.

The FEM analysis is carried out in two steps. In step one the detailed thermal stress distribution in the specimen due to a given temperature change is calculated. In the second step, the fibre is pulled out by the applied traction load. The fibre and the matrix in this step are subjected to the residual stresses obtained in step 1.

Slip at the matrix–fibre interface is allowed in both the initial thermal loading stage as well as in the applied traction loading stage.

The boundary conditions are as follows: in the residual stress calculation the axial displacement of the fibre and matrix nodes on the middle cross-section $z = t/2$ of the specimen are fixed because of symmetry; the rest of the specimen boundary is traction free. In the pull-out calculation, the matrix nodes on the boundary, $r = R_m$, are fixed to simulate a clamped condition for the matrix. The matrix and fibre nodes at the bottom of the specimen, $z = t$, are left traction free. The matrix nodes on $z = 0$ are traction free, whereas a uniform displacement, U_f, is applied to the fibre nodes.

To assess the accuracy of our FEM calculations, we applied our FEM model to analyse the fibre push-out

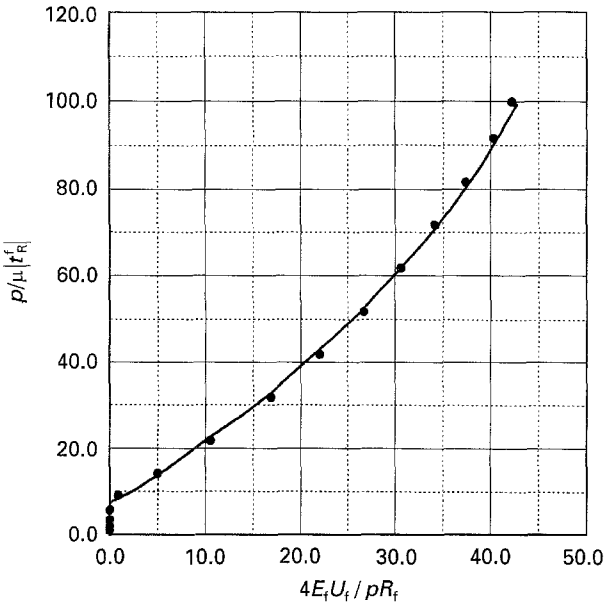

Figure 2 Comparison of (●) our FEM results for the case of the fibre push-out test with (—) the numerical results of Hoysan and Steif [24] for the case of $E_f/E_m = 3.54$, $\mu = 0.3$, $\nu_f = \nu_m = 0.3$. As in [24], the residual radial stress at the interface is modelled by the application of a constant pressure on the fibre and matrix interface elements.

test, which was carried out by Meda *et al.* [32]. This is done by reversing the loading on the fibre. Because Meda *et al.* [32], simulated the effect of thermal stress by the application of a constant pressure so that the axial residual stress is ignored, we did not carry out the initial thermal loading calculation but instead modelled the residual radial stress at the interface by the application of a constant pressure on the fibre and matrix interface elements. The axial residual stress is set equal to zero. The normalized displacement versus normalized load curve for the case of $E_f/E_m = 3.54$, $\mu = 0.3$, $\nu_f = \nu_m = 0.3$ is shown in Fig. 2 where the curve matches very well with the FEM analysis of Meda *et al.* [32]. The normalization used in this figure is identical to that reported elsewhere [32], and not that of Equation 20.

4. Numerical results

4.1. Thermal stress simulation

FEM thermal stress calculations were carried out to obtain the dependence of the residual stress distribution on the dimensionless parameters t/R_f, E_m/E_f and μ. To assess the accuracy of Equation 1, we normalized the calculated thermal stresses by the approximate thermal stress solution given by Equation 1

$$\bar{\sigma}_R = \frac{\sigma_R}{t_R^f} \tag{24a}$$

$$\bar{\sigma}_z = \frac{\sigma_z}{t_z^f} \tag{24b}$$

$$\bar{\sigma}_{Rz} = \frac{\sigma_{Rz}}{t_R^f} \tag{24c}$$

where t_R^f and t_z^f are given in Equation 1. Perfect agreement of the finite element results with the infinite fibre approximation given by Equation 1 would imply that $\bar{\sigma}_R = \bar{\sigma}_z = 1$ and $\bar{\sigma}_{Rz} = 0$.

In Figs 3–5 the normalized thermal stresses defined in the equations above are plotted as a function of the normalized axial position z/t. These calculations are carried out using different values of t/R_f, E_m/E_f and μ. The fixed parameters in these simulations are given by

$$E_f = 2.3 \times 10^{11} \text{ Pa} \tag{25a}$$

$$\nu_f = \nu_m = 0.3 \tag{25b}$$

$$\Delta\alpha\Delta T = 8 \times 10^{-4} \tag{25c}$$

As expected, the results of Figs 3–5 indicate that the infinite fibre approximation given by Equation 1 breaks down near the fibre ends, where slip of the fibre–matrix interface occurs due to thermal residual stresses. The size of these "thermal slip zones" and hence the accuracy of the infinite fibre assumption, depends on the parameters t/R_f, E_m/E_f and μ. Our simulation shows that the accuracy of the infinite fibre approximation improves as the parameters t/R_f, E_m/E_f and μ increase. Physically, this is easy to see, because a higher μ (as well as a higher radial stress) can allow the same amount of shear force to be transmitted across a smaller "thermal slip zone". We found that, for small friction coefficients ($\mu \sim 0.1$), a large thickness ratio $t/R_f \geqslant 100$ is needed to ensure the validity of the approximation of Equation 1.

4.2. Pull-out test simulation

Unless specified otherwise, simulations of the pull-out test were obtained using $t/R_f = 100$ to ensure the validity of the infinite fibre approximation for small friction coefficients. Also, all the finite element simulations in this section were carried out using the fixed set of parameters given by Equation 25a–c. Typically, simulations are performed to study the dependence of the pull-out test on the parameters E_m/E_f, μ, and the normalized displacement, $\bar{u}$.

The normalized displacement versus normalized load curve for the case of $E_m/E_f = 0.1$ and $\mu = 0.5$ is shown in Fig. 6. The curve, consisting of filled dots, is obtained using our FEM model. The curve consisting of open dots is obtained using the simplified FEM model where the effect of residual stress is replaced by a constant pressure applied on the interface. The solid line is obtained using Equation 21 with t_R^f and t_z^f given by Equation 1. The dashed line is obtained using Equation 21 with t_R^f given by Equation 1 and $t_z^f = 0$, which is the analytical solution for the case where the axial residual stress is neglected. This corresponds to the case of a constant pressure applied to the interface.

Fig. 6 shows that the normalized displacement is not zero at zero normalized load. Indeed, the analytical model, Equation 21, predicts that

$$\bar{u}_0 \equiv \bar{u}(\bar{p} = 0) = \frac{(1 - 2\nu_f k)}{2}\left(1 - \frac{1}{\bar{p}_{cr}}\right) \tag{26}$$

where we have used L'Hopital's rule to evaluate the limit as $p \to 0$ in Equation 21. Physically, the

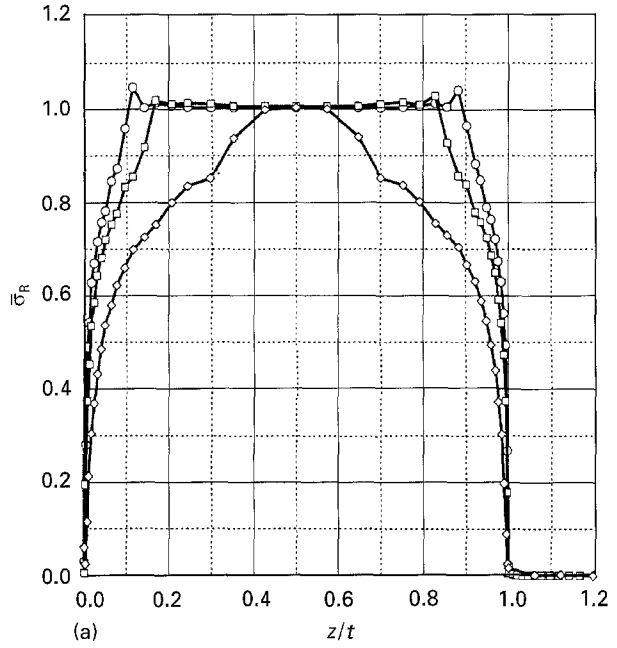

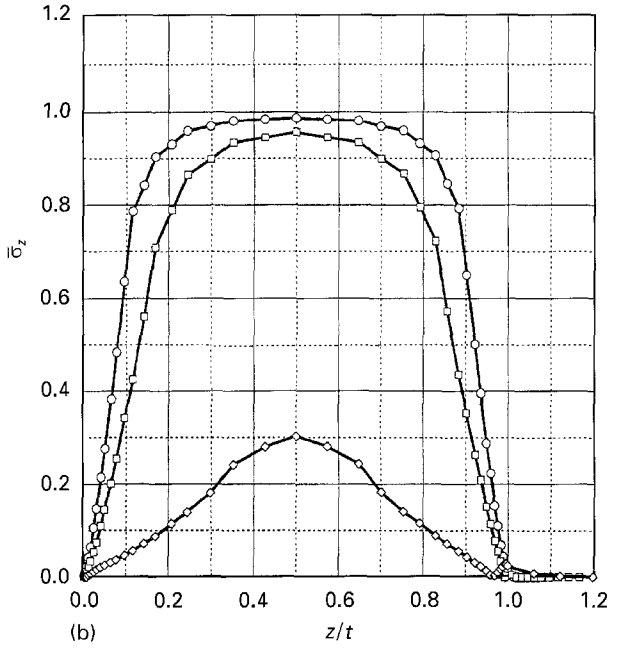

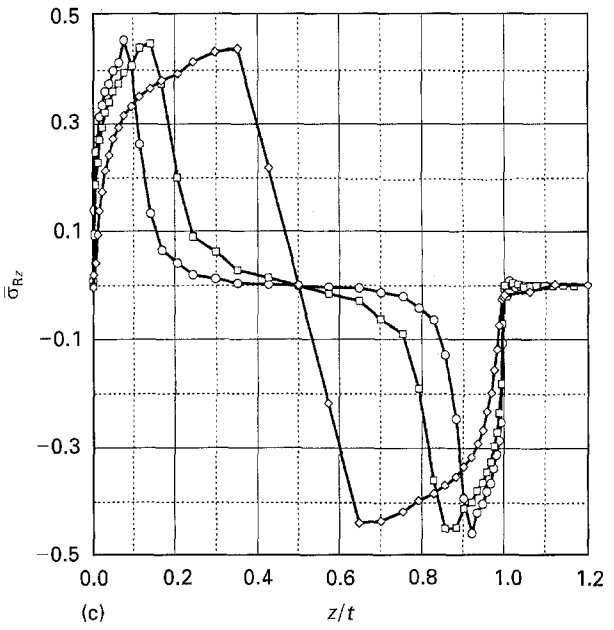

Figure 3 Comparison of (a) the thermal residual interface normal stress, (b) axial stress and (c) interface shear stress, which are obtained using FEM with those obtained using the infinite fibre approximation. This comparison is accomplished by using the normalized variables $\bar{\sigma}_R = \sigma_R/t_R^f$, $\bar{\sigma}_z = \sigma_z/t_z^f$, $\bar{\sigma}_{Rz} = \bar{\sigma}_{Rz}/t_z^f$. Perfect agreement of the finite element results with the infinite fibre approximation would imply that $\bar{\sigma}_R = \bar{\sigma}_z = 1$ and $\bar{\sigma}_{Rz} = 0$. These simulations were carried out using three different values of t/R_f = (●) 100, (□) 60 and (◇) 10 with $E_m/E_f = 0.1$, $\mu = 0.5$.

non-zero normalized displacement at zero applied load is caused by frictional slip induced by the axial thermal residual stress. Thus, the slope $d\bar{u}/d\bar{p}$ of the actual load–displacement curve is non-zero at zero load. On the other hand, Equation 26 predicts that $\bar{u}_0 = 0$ when the axial residual stress in the fibre is neglected because $\bar{p}_{cr} = 1$ in this case.

The results in Fig. 6 show that the analytical model agrees very well with the FEM. They also confirm the necessity of including the residual axial stress in the analysis, as pointed out elsewhere [29]. The curves given by the analytical model approach the normalized critical load $\bar{p}_{cr}$ (or $p_{cr} = t_z^f - (t_R^f/k)$), when the displacement becomes unbounded and the fibre slips with no friction. Note that the normalized critical load $\bar{p}_{cr} = 1$, for the case when the axial residual stress is set to zero (– – – in Fig. 6). In the FEM analysis, the slip zone eventually reaches the other end of the fibre (i.e. $L_S = t$). The friction force on the interface does not vanish when $L_S = t$ and the asymptotic value of the applied load is found to be slightly less than that predicted by p_{cr}. This is not surprising because the analytical model is derived assuming that $t = \infty$, whereas in the finite element model, a finite thickness is used. Our model gives $p_{cr} = t_z^f - (t_R^f/k)$, which is in good agreement with the results of the finite element analysis. It should be noted that Kerans and Parthasarathy [29] give p_{cr} in terms of a misfit strain. If we assume their misfit is due entirely to thermal stresses, then it can be expressed in terms of the residual stresses and is identical to our expression here. Also, one can show that, in the formulation of Li and Grubb [30], p_{cr} is identical to our expression if we set their debond length $l_d = \infty$ in their Equation 38 and if their misfit strain is expressed in terms of residual stresses.

The effect of the residual axial stress on the critical load is shown in Figs 7 and 8 for three different values of ν_f and E_m/E_f. These curves are obtained using the analytical model (Equation 21). The normalized critical load (i.e. the asymptotic value of the normalized load) is always 20%–30% lower than the unit value predicted by Equation 21 if the axial residual stress is set to be identically zero. Thus, the assumption of no axial residual stress overestimates the normalized critical load. It should be noted that, when the residual stress distribution differs significantly from the infinite fibre approximation (e.g. for $t/R_f = 10$), the finite element results given in Fig. 3 show that the axial residual stress is usually

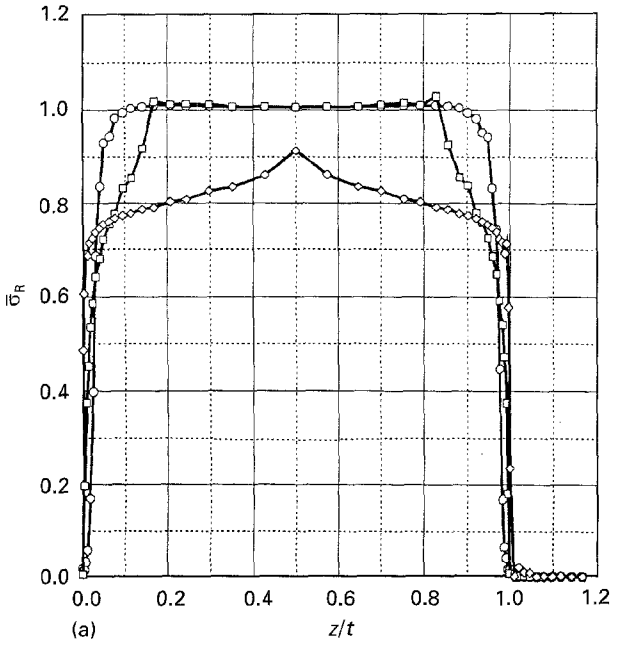

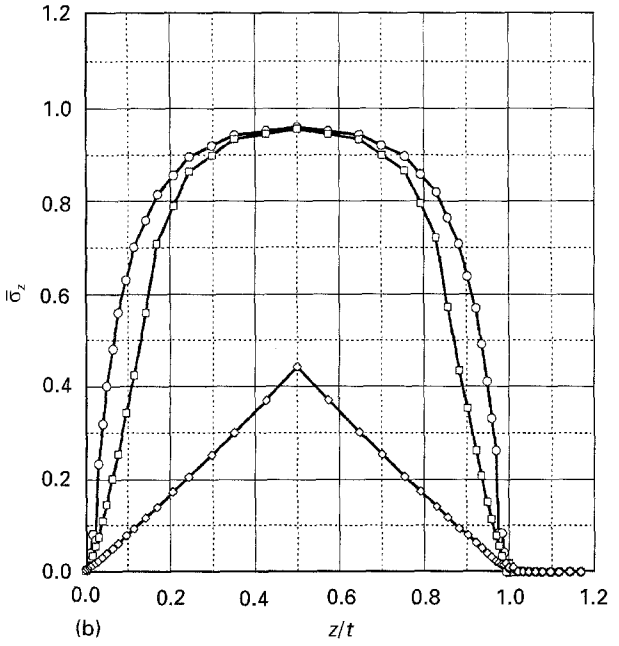

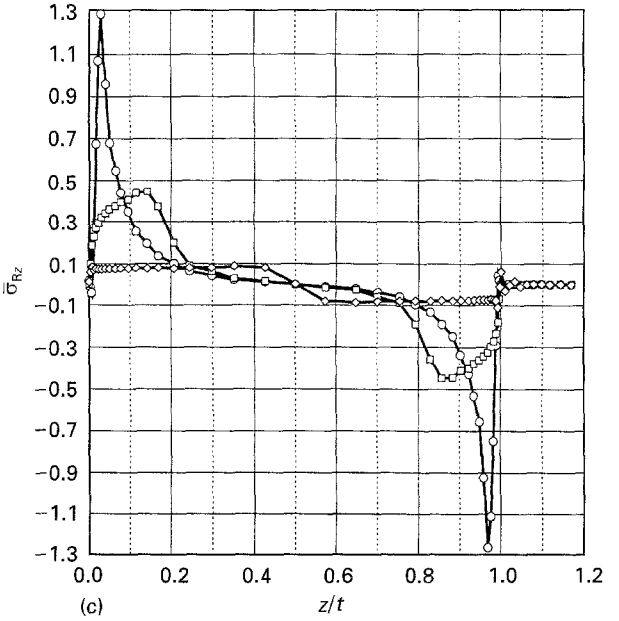

Figure 4 Comparison of (a) the thermal residual interface normal stress, (b) axial stress and (c) interface shear stress, obtained using FEM with those obtained using the infinite fibre approximation. This comparison is accomplished by using the normalized variables $\bar{\sigma}_R = \sigma_R/t_R^f$, $\bar{\sigma}_z = \bar{\sigma}_z/t_z^f$, $\bar{\sigma}_{Rz} = \bar{\sigma}_{Rz}/t_z^f$. Perfect agreement of the finite element results with the infinite fibre approximation would imply that $\bar{\sigma}_R = \bar{\sigma}_z = 1$ and $\bar{\sigma}_{Rz} = 0$. The simulations were carried out using three different values of friction coefficients $\mu = (\diamond)\ 0.1, (\square)\ 0.5$ and $(\bigcirc)\ 3.0$ with $E_m/E_f = 0.1$, $t/R_f = 60$.

much smaller than that predicted by Equation 1. We have also carried out finite element calculation for the case of $t/R_f = 10$ with $E_m/E_f = 1$ and $\mu = 0.1$. Our simulation shows that the thermal slip zone exceeds the thickness t. In this case, the analytical solution deviates significantly from the finite element result.

Figs 7 and 8 show the influence of ν_f and E_m/E_f on the pull-out test. The curves in these figures are generated using the analytical model Equation 21. The critical load decreases as the Poisson's ratio of the fibre and E_m/E_f increase. The results of the analytical model for $0.1 \leqslant E_m/E_f \leqslant 1$ are insensitive to variations of the matrix Poisson's coefficient, ν_m, and therefore are not shown here.

Next, we investigate the dependence of the pull-out test on the modulus ratio, E_m/E_f, and the friction coefficient, μ. Fig. 9 shows the results of the finite element analysis for $E_m/E_f = 0.3$ and $\mu = 0.1$ and 0.25. Results of the analytical model are shown in solid line. The results of the finite element analysis for the case of $E_m/E_f = 1.0$ with $\mu = 0.1$ and 0.25 are shown in Fig. 10. As in Fig. 9, the analytical solutions are also shown in solid line. Equation 21 implies that plots of normalized load versus normalized displacement should be independent of the friction coefficient, μ, this is confirmed by our FEM simulations in Figs 9 and 10. The agreement between the predictions of the analytical model and the finite element results is very good: within 5%–7% for $\mu = 0.25$ and within 2%–3% for $\mu = 0.1$.

The finite element results and the analytical solution for the interfacial shear (Equation 23a) inside the slip zone is shown in Fig. 11 for $\mu = 0.1$ and 0.5. The results for the axial fibre stress inside the slip zone for $\mu = 0.1$ and 0.5 are given in Fig. 12. These results are obtained using the same applied tension. They indicate that the agreement between the finite element and the approximate shear-lag analysis improves as the friction coefficient is reduced. One may expect that the agreement between the finite element and the approximate shear-lag analysis will depend only on the length of the slip zone. To check this hypothesis, we reduce the loading for the case of $\mu = 0.1$ so that the slip zone are of the same size as that of $\mu = 0.5$. The interfacial shear stress and the axial fibre stress obtained using this procedure are also shown in Figs 11 and 12. (The analytical solutions are given by the dotted lines and the finite element results by squares). Our results indicate that the lower the friction coefficient, the closer is the agreement between the finite element and the approximate shear-lag analysis even if

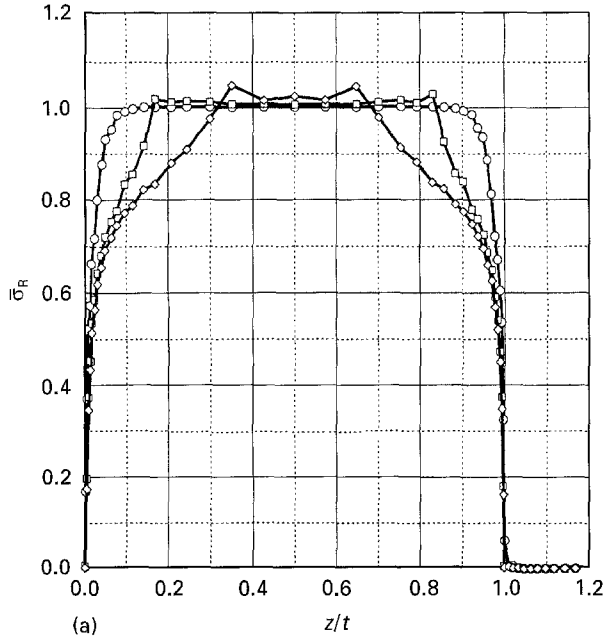

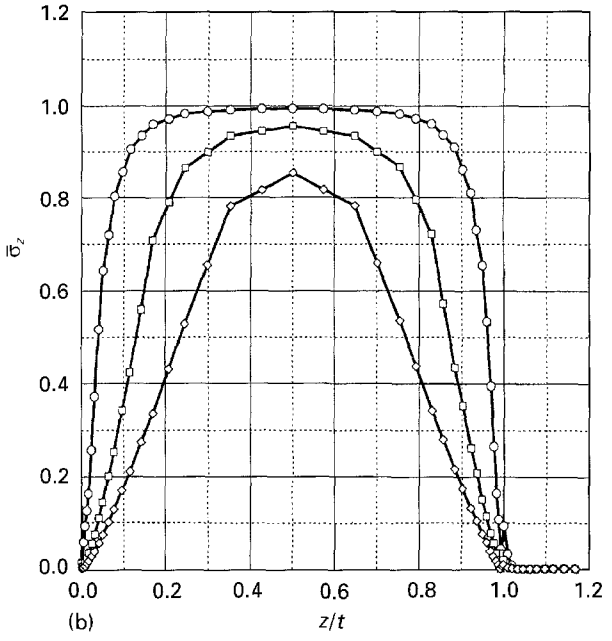

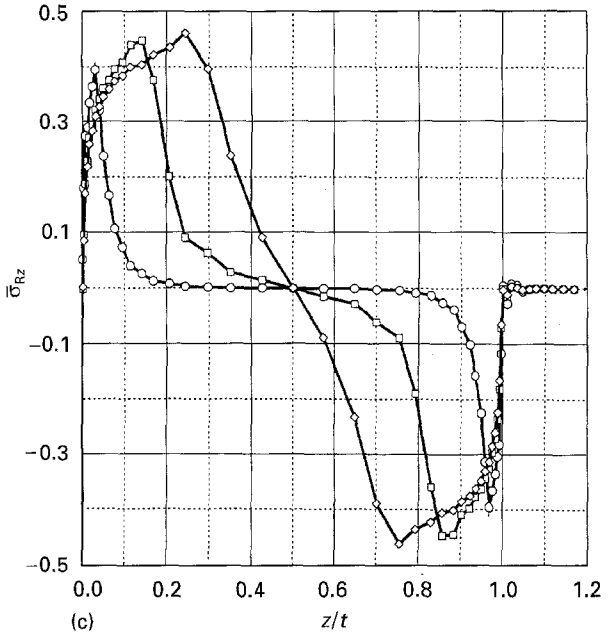

Figure 5 Comparison of (a) the thermal residual interface normal stress, (b) axial stress and (c) interface shear stress, obtained using FEM with those obtained using the infinite fibre approximation. This comparison is accomplished by using the normalized variables $\bar{\sigma}_R = \bar{\sigma}_R/t_R^f$, $\bar{\sigma}_z = \sigma_z/t_z^f$, $\bar{\sigma}_{Rz} = \sigma_{Rz}/t_z^f$. Perfect agreement of the finite element results with the infinite fibre approximation would imply that $\bar{\sigma}_R = \bar{\sigma}_z = 1$ and $\bar{\sigma}_{Rz} = 0$. The simulations were carried out using three different values of modulus ratio E_m/E_f = (○) 0.5, (□) 0.1 and (◇) 0.05 with $t/R_f = 60$ and $\mu = 0.5$.

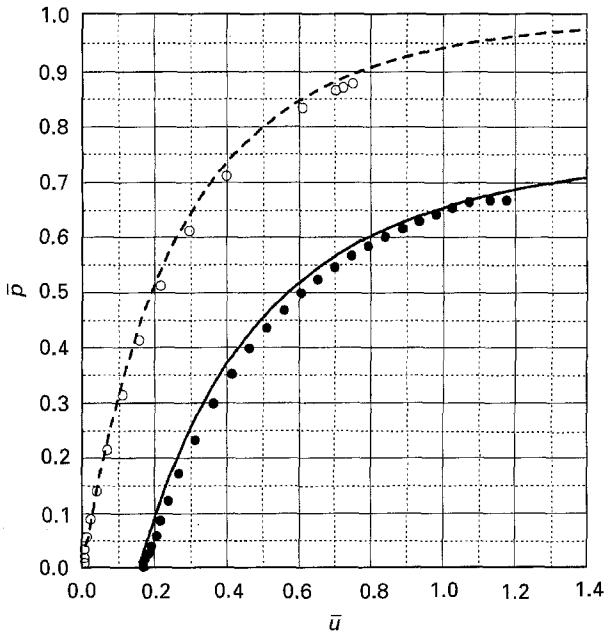

Figure 6 The normalized displacement $\bar{u} = (\mu k E_f/pR_f)\, U_f$ versus normalized load $\bar{p} = (k/|t_R^f|)\, p$ curve for the case of $E_m/E_f = 0.1$, $\mu = 0.5$. (●) curve obtained using our FEM model; (○) curve obtained using the simplified FEM model where the effect of residual stress is replaced by a constant pressure applied on the interface. (—) curve obtained using the analytical solution, Equation 21, with t_R^f and t_z^f given by Equation 1. (– – –) curve obtained using Equation 21 with t_R^f given by Equation 1 and $t_z^f = 0$, which is the analytical solution. This corresponds to the case of a constant pressure applied to the interface for the case where the axial residual stress is neglected.

the slip zones are of the same size. It should be noted that the agreement between the approximate shear-lag analysis and the finite element results for the load versus displacement curve is much less sensitive to the friction coefficient, as pointed out above.

5. Discussion and conclusion

Our finite element simulation shows that there is excellent agreement between our approximated analytical solution, which is based on a shear-lag analysis. For example, the displacement versus load relation given by Equation 21, as well as the critical load for complete fibre pull-out, compares very well with the finite element results. The analytical model is accurate for μ in the range $0.5 \geqslant \mu \geqslant 0.1$, although it could be accurate for a larger set of μ. The dependence of the pull-out force on the elastic modulus of the matrix and fibre is also well approximated by the analytical model. The interfacial shear stress and the fibre stress is also accurately predicted by the shear-lag model provided that μ is small. Thus the shear lag model

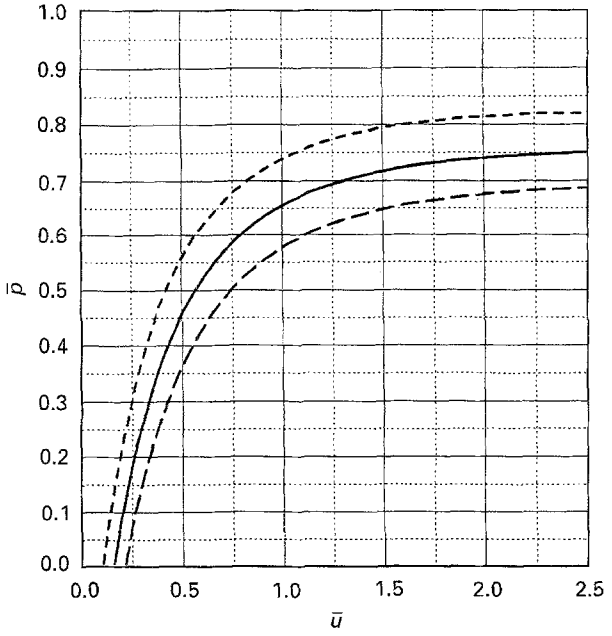

Figure 7 The dependence of the normalized displacement $\bar{u} = (\mu k E_f / p R_f)\, U_f$ versus normalized load $\bar{p} = (k/|t_R^f|)\, p$ curve on the Poisson's ratio of the fibre: (- - -) 0.2, (—) 0.3, (— — —) 0.4.

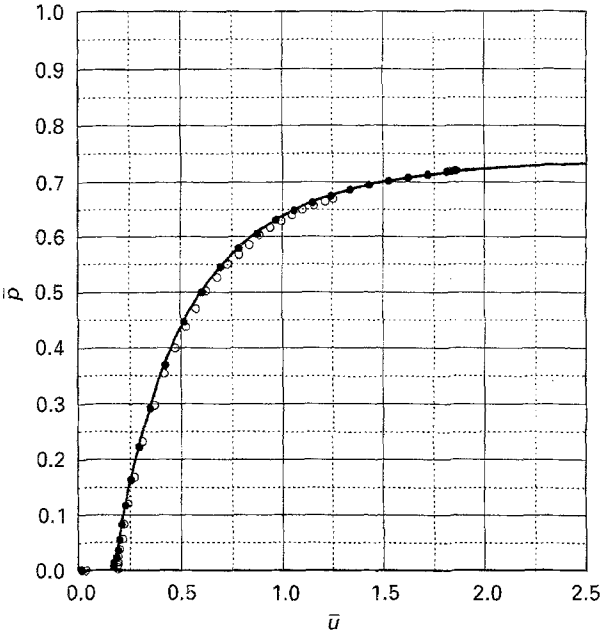

Figure 9 Comparison of the normalized displacement versus normalized load curve obtained by finite element results with those obtained by the analytical model (Equation 21) for two different μ with $E_m/E_f = 0.3$. (●) $\mu = 0.1$, (○) $\mu = 0.25$.

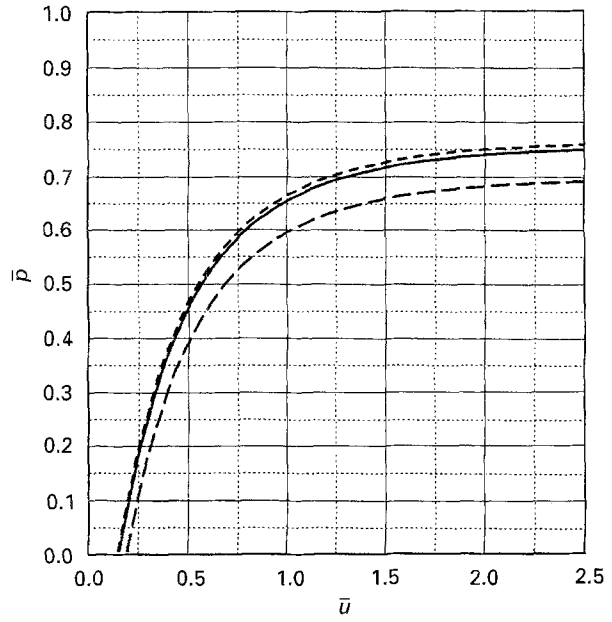

Figure 8 The dependence of the normalized displacement $\bar{u} = (\mu k E_f / p R_f)\, U_f$ versus normalized load $\bar{p} = (k/|t_R^f|)\, p$ curve on the modulus ratio E_m/E_f: (- - -) 0.001, (—) 0.1, (— — —) 1.0.

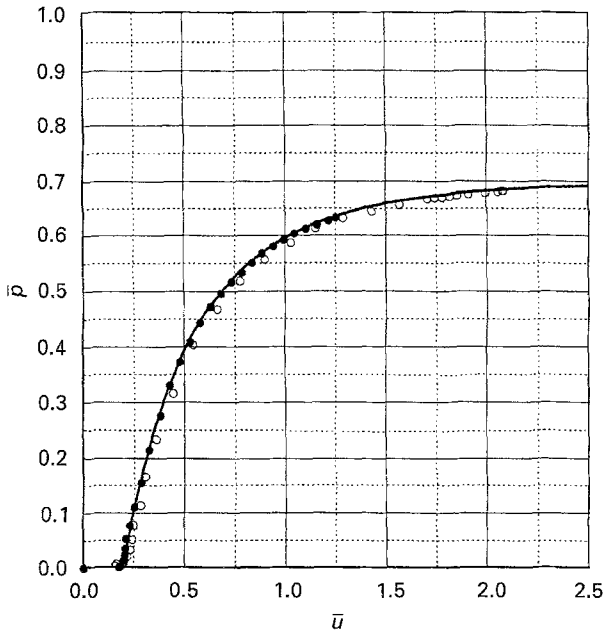

Figure 10 Comparison of the normalized displacement versus normalized load curve obtained by finite element results with those obtained by the analytical model (Equation 21) for two different μ with $E_m/E_f = 1$. (●) $\mu = 0.1$, (○) $\mu = 0.25$.

captures accurately all the relevant features of the pull-out test provided that the following conditions are satisfied.

1. The accuracy of the analytical solution depends on the ratio t/R_f. The thermal residual stresses are accurately predicted by the infinite fibre approximation for friction coefficient $\mu \geqslant 0.1$ as long as $t/R_f \geqslant 100$. When t/R_f is sufficiently small so that the thermal slip zone occupies a significant portion of the fibre–matrix interface, the agreement between the finite element simulation and the analytical solution is very poor.

2. The effect of residual axial stress should be included in models of fibre pull-out. Our finite element result shows that the interface can slip before load application. This leads to non-zero fibre displacement at zero load. Furthermore, the critical load for complete pull-out of the fibre is overestimated by about 30% if the axial residual stress is neglected in the modelling.

3. The fibre stress and the interfacial stress inside the slip zone is accurately predicted by the shear-lag model. As expected, the smaller the friction coefficient, the better is the shear-lag approximation. The displacement versus load relation is much less sensitive to the friction coefficient. Our finite element results show

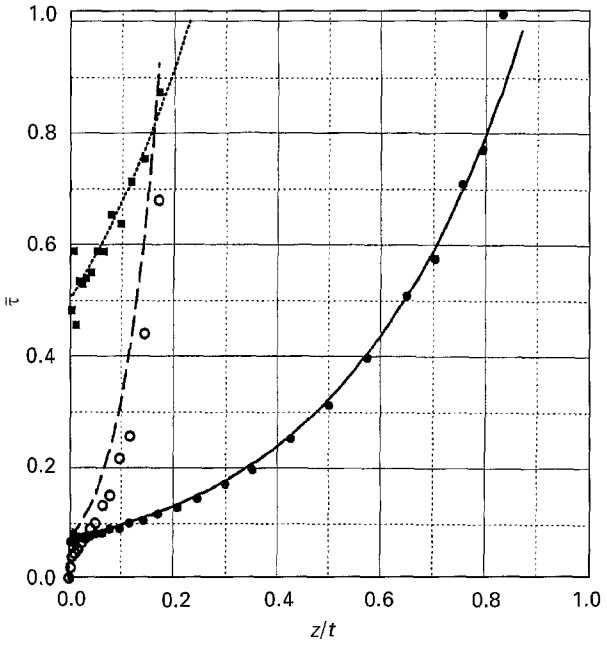

Figure 11 The normalized interface shear stress $\bar{\tau} \equiv \sigma_{Rz}/\mu|t_R^f|$ inside the slip zone for two different friction coefficients $\mu = 0.1$ and 0.5 with $E_m/E_f = 1$. The finite element results for: (●) $\mu = 0.1$, $\bar{p} = 0.63$, (○) $\mu = 0.5$, $\bar{p} = 0.63$, and (■) $\mu = 0.1$, $\bar{p} = 0.20$. Predictions of the analytical model: (—) $\mu = 0.1$, $\bar{p} = 0.63$, (– – –) $\mu = 0.5$, $\bar{p} = 0.63$, and (···) $\mu = 0.1$, $\bar{p} = 0.20$; ($\bar{p}$) indicates the normalized load used in the simulation.

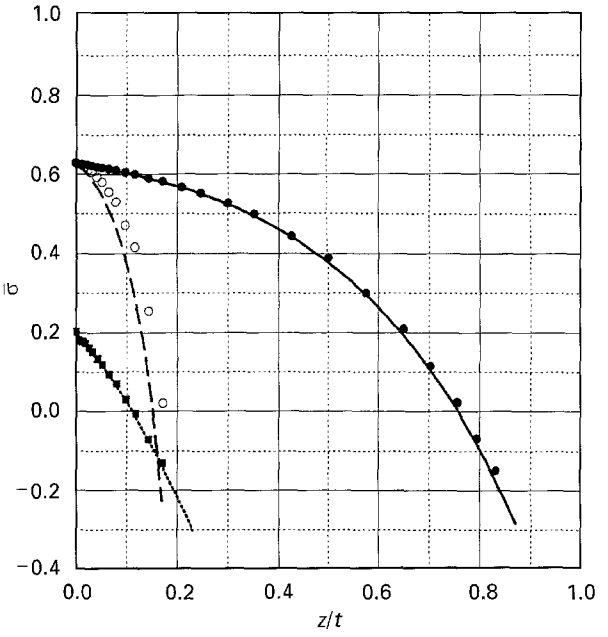

Figure 12 The normalized axial fibre stress $\bar{\sigma} \equiv (\bar{p}_{cr} - \bar{\tau})$ inside the slip zone for two different friction coefficients $\mu = 0.1$ and 0.5 with $E_m/E_f = 1$. The finite element results: (●) $\mu = 0.1$, $\bar{p} = 0.63$, (○) $\mu = 0.5$, $\bar{p} = 0.63$, and (■) $\mu = 0.1$, $\bar{p} = 0.20$. Predictions of the analytical model: (—) $\mu = 0.1$, $\bar{p} = 0.63$, (– – –) $\mu = 0.5$, $\bar{p} = 0.63$, and (···) $\mu = 0.1$, $\bar{p} = 0.20$. ($\bar{p}$) The normalized load used in the simulation.

that the fibre displacement is inversely proportional to the friction coefficient.

Although the procedure of our analytical solution differs somewhat from that of Kerans and Parthasarathy [29] and Li and Grubb [30], many of their expressions are practically identical to ours provided that their misfit strain is expressed in terms of the thermal residual stresses. We note that Li and Grubb [30] did not give a displacement versus load relation, as they were mainly interested in measuring the interfacial stress using Raman spectrometry. Thus, the analytical analysis of these authors (and perhaps others) is also an accurate description of the pull-out test.

In this work the fibre–matrix interface was modelled by Coulomb friction. We have not considered interface models that described debonding accompanied by frictional slip. Approximate analytical solution of the pull-out test using these interface models can be found elsewhere [26, 27].

Acknowledgements

This work was promoted by an exchange agreement between ENEA (Area Energia ed Innovazione) and Cornell University (College of Engineering). The work by A. Zucchini was supported in part by the CETMA project which is funded by the STRIDE programme of the EC. C. Y. Hui was supported in part by the Material Science Center which is funded by the National Science Foundation (DMR-MRL programme). C. Y. Hui also acknowledges the support of the Air Force Office of Scientific Research under Contract F49620-931-0235.

References

1. J. AVESTON, G. A. COOPER and A. KELLY, in "The Properties of Fibre Composites", Conference Proceedings, National Physical Laboratory, Guildford (IPC Science and Technology Press, Teddington, 1971) 15.
2. W. A. FRASER, F. H. ANCKER, A. T. DIBENEDETTO and B. ELBIRLI, *Polym. Compos.* **4** (1983) 238.
3. A. N. NETRAVALI, R. B. HENSTENBURG, S. L. PHOENIX and P. SCHWARTZ, *ibid.* **10** (1989) 226.
4. D. B. MARSHALL, *J. Am. Ceram. Soc.* **67** (1984) C-259.
5. D. K. SHETTY, *ibid.* **71** (1988) C-107.
6. A. DOLLAR, P. S. STEIF, Y. C. WANG and C. Y. HUI, *Int. J. Solids Struct.* **30** (1993) 1313.
7. C. LIANG and J. W. HUTCHINSON, *Mech. Mater.* **14** (1993) 207.
8. L. J. BROUTMAN, in "Interfaces in Composites" ASTM STP 452, edited by M. L. Salkind (American Society for Testing and Materials, Philadelphia, PA, 1969) p. 27.
9. J.-P. FAVRE and M. C. MERIENNE, *Int. J. Adhes. Adhes.* **1** (1981) 311.
10. D. B. EAGLES, B. F. BLUMENTRITT and S. L. COOPER, *J. Appl. Polym. Sci.* **20** (1976) 435.
11. L. S. PENN and S. M. LEE, *J. Compos. Technol. Res.* **11** (1989) 23.
12. G. DESARMOT and J.-P. FAVRE, *Compos. Sci. Technol.* **42** (1991) 151.
13. H. L. COX, *Br. J. Appl. Phys.* **3** (1952) 72.
14. J. AVESTON and A. KELLY, *J. Mater. Sci.* **8** (1973) 352.
15. L. N. McCARTNEY, *Proc. R. Soc. Lond.* **A425** (1987) 215.
16. B. BUDIANSKY, J. W. HUTCHINSON and A. G. EVANS, *J. Mech. Phys. Solids* **34** (1986) 167.
17. L. B. GRESZCZUK, in "Interfaces in Composites", ASTM STP 452 (American Society for Testing and Materials, Philadelphia, PA, 1969) p. 42.
18. P. LAWRENCE, *J. Mater. Sci.* **7** (1972) 1.
19. A. TAKAKU and R. G. C. ARRIDGE, *J. Phys. D Appl. Phys.* **6** (1973) 2038.
20. P. BARTOS, *J. Mater. Sci.* **15** (1980) 3122.
21. R. J. GRAY, *ibid.* **19** (1984) 861.

22. P. S. CHUA and M.R. PIGGOTT, *Compos. Sci. Technol.* **22** (1985) 33.
23. A. V. SARMA, P. N. MURTHY and P. S. KUSHWAHA, *Fiber Sci. Technol.* **12** (1979) 129.
24. P. STEIF and S. F. HOYSAN, *Mech. Mater.* **5** (1986) 375.
25. L. S. SIGL and A. G. EVANS, *ibid.* **8** (1989) 1.
26. Y. C. GAO, Y.-W. MAI and B. COTTERELL, *J. Appl. Math and Phys. (ZAMP)* **39** (1988) 550.
27. J. W. HUTCHINSON and H. M. JENSEN, *Mech. Mater.* **9** (1990) 139.
28. D. B. MARSHALL, *Acta Metall. Mater.* **40** (1992) 427.
29. R. J. KERANS and T.A. PARTHASARATHY, *J. Am. Ceram. Soc.* **74** (1991) 1585.
30. Z.-F. LI and D. T. GRUBB, *J. Mater. Sci.* **29** (1994) 189.
31. M. UEMURA, H. IYAMA and Y. YAMAGUCHI, *J. Thermal Stresses* **2** (1979) 393.
32. G. MEDA, S. F. HOYSAN and P. STEIF, *J. Appl. Mech.* **60** (1993) 986.

Received 10 August 1995
and accepted 24 April 1996